DOI 10.5162/IMCS2012/P2.0.20

# Enhancing *p*-type $Co_3O_4$ Gas Sensing Performances by Fluorine Doping

*D. Bekermann[1], A. Gasparotto[1], D. Barreca[2], C. Maccato[1], E. Comini[3], M. Gavagnin[1], C. Sada[4], G. Sberveglieri[3], A. Devi[5], R. A. Fischer[5]*
*[1] Department of Chemistry, Padova University and INSTM, 35131 Padova, Italy*
*daniela.bekermann@unipd.it*
*[2] CNR-ISTM and INSTM, Department of Chemistry, Padova University, 35131 Padova, Italy*
*[3] CNR-IDASC, SENSOR Lab, Department of Chemistry and Physics, Brescia University, 25133 Brescia, Italy*
*[4] Department of Physics and CNISM, Padova University, 35131 Padova, Italy*
*[5] Lehrstuhl für Anorganische Chemie II, Ruhr-University Bochum, 44780 Bochum, Germany*

**Abstract:**
In the present work, $Co_3O_4$-based materials were grown by Plasma Enhanced-Chemical Vapor Deposition (PE-CVD) and tested in the detection of reducing analytes (ethanol, acetone). In particular, $Co_3O_4$ and F doped $Co_3O_4$ deposits were synthesized in the range 200-400°C on polycrystalline $Al_2O_3$ substrates from Ar-$O_2$ plasmas using $Co(dpm)_2$ (dpm = 2,2,6,6-tetramethyl-3,5-heptanedionate) and $Co(hfa)_2$·TMEDA (hfa = 1,1,1,5,5,5-hexafluoro-2,4-pentanedionate; TMEDA = *N*,*N*,*N'*,*N'*-tetramethylethylenediamine), respectively. In the latter case, a homogeneous fluorine doping throughout the whole deposit thickness was achieved, and its content could be controlled as a function of the deposition temperature. Notably, the sensing performances appreciably improved upon fluorine incorporation into cobalt oxide. To the best of our knowledge, this work is the first example of F doping in *p*-type metal oxide nanosystems aimed at enhancing their sensing properties.

**Key words:** Plasma Enhanced-Chemical Vapor Deposition, fluorine doping, $Co_3O_4$, gas sensors

## Introduction

In the last decade, the need for ever improved sensor devices, stimulated by the rising environmental pollution and by health/safety issues, has biased the attention of the scientific community towards the fabrication of novel nanostructured materials with high surface area and tailored electrical properties. [1-3] In this context, at variance from the widely investigated *n*-type semiconductors (SCs), the use of oxide-based *p*-type materials paves the way to the exploration of novel gas sensing patterns that can enhance sensitivity/selectivity in the detection of different molecular species. [1,4-5] Among *p*-type oxides, $Co_3O_4$ is a well-known catalyst for various oxidation processes, but its surface reactivity and defectivity have been seldom exploited for gas sensing applications. [1,2,5-7] The possibility to further modify the functional properties of this *p*-type SC by a tailored anion doping appears as a versatile tool to enhance its response toward the target gases. In this framework, fluorine incorporation into $Co_3O_4$ may improve its gas sensing performances by increasing the Lewis-acidity of the cobalt centres and saturating dangling bonds at the surface, whose presence is detrimental for the trapping of free carriers. [1,8-10]

In the present work, we report on the development of pure and fluorine doped $Co_3O_4$-based sensor materials, investigating the impact of anion doping on the detection of acetone and ethanol, of interest for biomedical/food industries and the development of breath analyzers. [11-13]

## Experimental

Undoped and fluorine doped $Co_3O_4$ deposits were grown on polycrystalline alumina slides from $Co(dpm)_2$ (**Co1**) [14] and $Co(hfa)_2$·TMEDA (**Co2**) [15], respectively, using a two-electrode Radio Frequency (RF; $\nu$ = 13.56 MHz) PE-CVD apparatus. [16] The precursors **Co1** and **Co2**, placed in an external bubbler, were vaporized at 60°C and 90°C, and transported into the reaction chamber by a 60 sccm Ar flow. Additional Ar and $O_2$ flows (rates = 15 and 20

sccm) were directly introduced into the reaction system. Depositions were carried out at temperatures between 200 and 400°C at a fixed total pressure, RF-power, and process duration of 1.0 mbar, 20 W, and 1 h.

Glancing Incidence X-Ray Diffraction (GIXRD) patterns were recorded by means of a Bruker D8 Advance diffractometer equipped with a Göbel mirror and a Cu Kα source (40 kV, 40 mA), at a fixed incidence angle of 3.0°. Field Emission Scanning Electron Microscopy (FE-SEM) micrographs were collected at a primary beam acceleration voltage of 5.0 kV by a Zeiss SUPRA 40VP instrument. Atomic Force Microscopy (AFM) analyses were performed using a NT-MDT SPM Solver P47HPRO instrument operating in tapping mode and in air. Root-mean-square (RMS) roughness values were obtained from 10 $\mu m^2$ images after background subtraction. Secondary Ion Mass Spectrometry (SIMS) measurements were carried out using a IMS 4f mass spectrometer with a $Cs^+$ primary beam (14.5 keV, 10 nA). Depth profiles were recorded rastering over a 150 µm × 150 µm area and collecting negative secondary ions from a sub-region close to 8 µm × 8 µm to avoid crater effects, adopting charge neutralization by means of an electron gun.

Gas sensing analyses were carried out by the flow-through technique in a temperature stabilized sealed chamber at 1 atm, 20°C and constant humidity level (40%). Synthetic air from certified bottles (flow = 0.3 $l \times min^{-1}$) was used as a carrier gas. [17] For sensor fabrication, 200 µm-spaced Pt electrodes and a Pt heater were sputtered on the composite materials surface and on the backside of the $Al_2O_3$ substrates, respectively. A constant bias voltage of 1 V was applied to the specimens and the flowing current was measured through a picoammeter. Before gas sensing tests, each sample was pre-stabilized at the desired working temperature (200–400°C) for 8 h. The sensor response (uncertainty = ±5%) was defined according to eq. (1): [1,11,17,18]

$$S = \frac{R_f - R_0}{R_0} = \frac{\Delta R}{R} \qquad (1)$$

where $R_0$ and $R_f$ are the baseline resistance values measured in air and the steady state value reached upon gas exposure, respectively.

## Results

The structure and morphology of the synthesized deposits, investigated by GIXRD, FE-SEM and AFM analyses, were very similar for all $Co_3O_4$ specimens grown from both **Co1** and **Co2**. In particular, GIXRD revealed the formation of the cubic $Co_3O_4$ phase, irrespective of the used precursor and the adopted processing parameters. [1,19] Nanocrystal diameters (d) of ≈ 30 nm were estimated by the Scherrer equation.

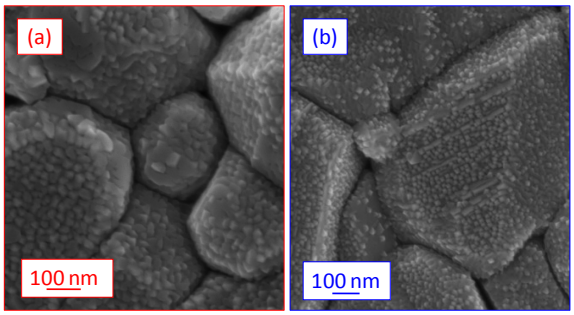


*Fig. 1. Plane-view FE-SEM micrographs for undoped (a) and fluorine doped (b) $Co_3O_4$ specimens deposited at 300°C from **Co1** and **Co2**, respectively.*

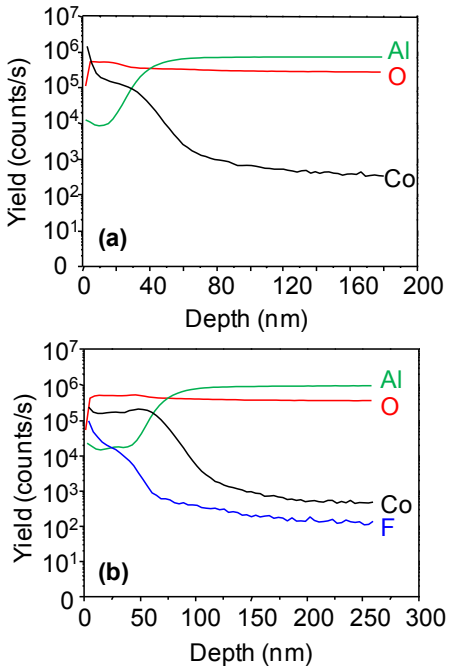


*Fig. 2. SIMS depth profiles for undoped (a) and fluorine doped (b) $Co_3O_4$ specimens deposited at 200°C starting from **Co1** and **Co2**, respectively. Adapted from [1].*

Plane-view FE-SEM micrographs (Fig. 1) evidenced the presence of $Al_2O_3$ globular particles (average diameter ≈ 600 nm) uniformly covered by small pyramidal-like $Co_3O_4$ nanoaggregates with an average size of ≈ 30 nm, in line with GIXRD measurements. As a matter of fact, the faceting detected for $Co_3O_4$ particles is typical for face-centered cubic systems exposing low surface energy planes. [20] The conformal coverage of the alumina substrate by cobalt oxide resulted in a very rough surface morphology (RMS roughness ≈ 75 nm) for all the investigated specimens, as evidenced by AFM measurements. Overall, the

uniform dispersion of $Co_3O_4$ nanoparticles on the substrate surface and the low crystallite size likely result in a high active area, an advantageous feature for gas sensing applications. [1,12,13]

The main difference between deposits synthesized from the two precursors regarded their chemical composition, as highlighted by SIMS analyses (Fig. 2). Indeed, while **Co1** yielded pure $Co_3O_4$, in the case of **Co2** specimens were characterized by an homogeneous fluorine doping from the surface up to the interface with the substrate, an effect that could be explained by the generation of stable $F^{\bullet}$ radicals in the used plasmas. [21] In particular, the almost parallel trend of Co and O ionic yields in Fig. 2a pointed out to the presence of $Co_3O_4$ as the only cobalt-containing phase, in line with GIXRD results. In the case of samples obtained from $Co(hfa)_2{\cdot}TMEDA$ (**Co2**), this feature was also accompanied by the presence of fluorine (Fig. 2b), whose ionic yield strongly resembled the trend detected for Co signal. It is also worthwhile noting that the fluorine content decreased with increasing deposition temperature from 200 to 400°C.

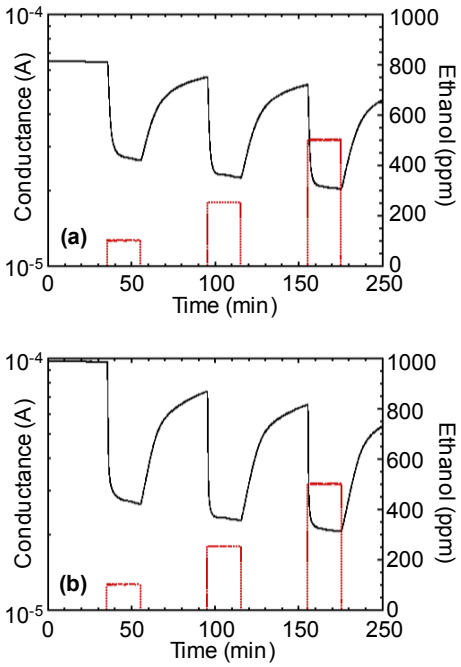


*Fig. 3. Conductance variations (sensor working temperature = 200°C) upon exposure to ethanol square concentration pulses (100, 250 and 500 ppm) for undoped (a) and fluorine doped (b) $Co_3O_4$ specimens deposited at 200°C from **Co1** and **Co2**, respectively.*

Fig. 3 displays the conductance variation detected for two representative undoped and F doped $Co_3O_4$ sensors upon exposure to ethanol. In both cases, no saturation effects were observed, as indicated by the higher conductance modulation revealed upon increasing ethanol concentration. Notably, a comparison of Fig. 3a and Fig. 3b highlights enhanced conductance variations for F-$Co_3O_4$ than for pure $Co_3O_4$ under same experimental conditions, pointing out to a beneficial influence of fluorine doping on the sensor performances.

As a matter of fact, control of F doping level as a function of the processing parameters revealed to be the key issue to tune the gas sensing performances of the present $Co_3O_4$-based materials.

To this regard, Fig. 4 compares F doped $Co_3O_4$ sensors with different fluorine contents in the detection of acetone. As can be observed, irrespective of the target gas concentration, the highest responses were always obtained for the sample synthesized at the lowest growth temperature, *i.e.* for the material characterized by the highest fluorine content. This behavior was traced back to: (i) the high fluorine electronegativity, enhancing the Lewis acidity and catalytic activity of Co centers; (ii) the saturation of dangling bonds at the sensor surface, increasing thus the concentration of holes directly involved in the sensing process. [1,8-10]

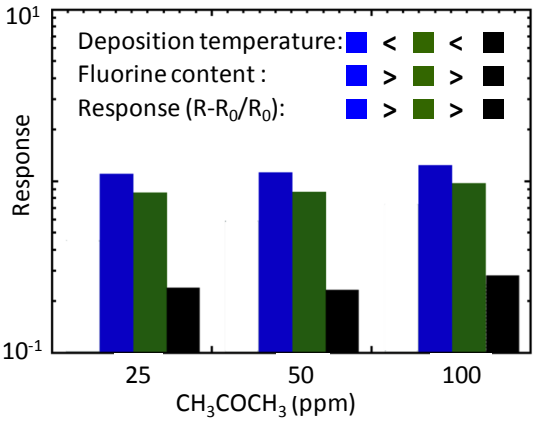


*Fig. 4. Responses to various acetone concentrations (sensor working temperature = 200°C) obtained from F-$Co_3O_4$ specimens deposited at 200°C (blue), 300°C (green) and 400°C (black).*

## Conclusions

In summary, a one-step PE-CVD process to F doped $Co_3O_4$ has been developed and optimized to tailor fluorine content in the target material. Gas sensing tests aimed at the detection of acetone and ethanol revealed that fluorine doped samples display responses appreciably higher that undoped $Co_3O_4$, an attractive feature for the fabrication of innovative sensor devices. [1,22] To the best of our knowledge, this work is the first study on *in-situ* fluorine doping of *p*-type $Co_3O_4$ for gas

sensing applications. The presented results are expected to add novel information to the research towards improved *p*-type sensing materials.

**Acknowledgements**

The research leading to these results has received funding from the European Community's Seventh Framework Program (FP7/2007-2013; Grant Agreement n° ENHANCE-238409) and Padova University PRAT 2010 project (n° CPDA102579).

**References**

[1] D. Barreca, D. Bekermann, E. Comini, A. Devi, R. A. Fischer, A. Gasparotto, M. Gavagnin, C. Maccato, C. Sada, G. Sberveglieri, E. Tondello, *Sens. Actuators, B* 160, 79−86 (2011)

[2] D. Bekermann, A. Gasparotto, D. Barreca, C. Maccato, E. Comini, C. Sada, G. Sberveglieri, A. Devi, R. A. Fischer, *ACS Appl. Mater. Interfaces* 4, 928−934 (2012)

[3] E. Comini, G. Sberveglieri, *Mater. Today* 13, 28–36 (2010)

[4] J. Park, X. Shen, G. Wang, *Sens. Actuators, B* 136, 494–498 (2009)

[5] J. Wöllenstein, M. Burgmair, G. Plescher, T. Sulima, J. Hildenbrand, H. Bottner, I. Eisele, *Sens. Actuators, B* 93, 442–448 (2003)

[6] D. Barreca, E. Comini, A. Gasparotto, C. Maccato, A. Pozza, C. Sada, G. Sberveglieri, E. Tondello, *J. Nanosci. Nanotechnol.* 10, 8054-8061 (2010)

[7] K.-I. Choi, H.-R. Kim, K.-M. Kim, D. Liu, G. Cao, J.-H. Lee, *Sens. Actuators, B* 146, 183-189 (2010)

[8] Y. Zhao, X. Du, X. Wang, J. He, Y. Yu, H. He *Sens. Actuators., B* 151, 205-211 (2010)

[9] B. Liu, M. Gu, X. Liu, S. Huang, C. Ni, *Appl. Phys. Lett.* 97, 122101 (2010)

[10] H. Y. Xu, Y. C. Liu, R. Mu, C. L. Shao, Y. M. Lu, D. Z. Shen, X. W. Fan, *Appl. Phys. Lett.* 86, 123107 (2005)

[11] D. Barreca, E. Comini, A. Gasparotto, C. Maccato, C. Sada, G. Sberveglieri, E. Tondello, *Sens. Actuators., B* 141, 270-275 (2009)

[12] C. C. Li, X. M. Yin, T. H. Wang, H. C. Zeng, *Chem. Mater.* 21, 4984–4992 (2009)

[13] D. Barreca, D. Bekermann, E. Comini, A. Devi, R. A. Fischer, A. Gasparotto, C. Maccato, C. Sada, G. Sberveglieri, E. Tondello, *CrystEngComm* 12, 3419–3421 (2010)

[14] D. Barreca, C. Massignan, S. Daolio, M. Fabrizio, C. Piccirillo, L. Armelao, E. Tondello, *Chem. Mater*. 13, 588–593 (2001)

[15] G. Bandoli, D. Barreca, A. Gasparotto, C. Maccato, R. Seraglia, E. Tondello, A. Devi, R. A. Fischer, M. Winter, *Inorg. Chem*. 48, 82–89 (2009)

[16] D. Barreca, A. Gasparotto, E. Tondello, C. Sada, S. Polizzi, A. Benedetti, *Chem. Vap. Deposition* 9, 199–206 (2003)

[17] D. Barreca, A. Gasparotto, C. Maccato, C. Maragno, E. Tondello, E. Comini, G. Sberveglieri, *Nanotechnol.* 18, 125502 (2007)

[18] S. D. Choi, B. K. Min, *Sens. Actuators, B* 77, 330–334 (2001)

[19] JCPDS, pattern n$^{o}$ 42-1467, 2000

[20] D. Barreca, A. Gasparotto, O. I. Lebedev, C. Maccato, A. Pozza, E. Tondello, S. Turner, G. Van Tendeloo, *CrystEngComm* 12, 2185-2197 (2010)

[21] A. Gasparotto, D. Barreca, D. Bekermann, A. Devi, R. A. Fischer, P. Fornasiero, V. Gombac, O. I. Lebedev, C. Maccato, T. Montini, G. Van Tendeloo, E. Tondello, *J. Am. Chem. Soc*. 133, 19362–19365 (2011)

[22] J. Park, X. Shen, G. Wang, *Sens. Actuators, B* 136, 494–498 (2009)